JOURNAL OF AIRCRAFT
Vol. 46, No. 6, November–December 2009

Improved Representation of High-Lift Devices for a Multidisciplinary Conceptual Aircraft Design Process

Christian Werner-Spatz,* Wolfgang Heinze,† and Peter Horst‡
Technische Universitaet Braunschweig, 38108 Braunschweig, Germany

DOI: 10.2514/1.42845

A methodology for improving the quality of high-lift-system performance prediction within a multidisciplinary conceptual design process is presented. The high-lift-system geometry is explicitly modeled and a multiple-lifting-line method is used to compute its aerodynamic characteristics. Computation times are acceptable for use in a conceptual design process. The results for several test cases show good agreement with wind-tunnel and/or high-fidelity numerical data. In addition, the method allows for further enhancement by using nonlinear airfoil polars for interpolation, improving drag prediction, and introducing some degree of nonlinear aerodynamic behavior.

Nomenclature

A	=	altitude
A'	=	numerical coefficient
B'	=	numerical coefficient
C_D	=	drag coefficient (3-D)
C_{Di}	=	induced drag coefficient (3-D)
C_{D0}	=	zero-lift drag coefficient (3-D)
C_d	=	section drag coefficient (2-D)
C_L	=	lift coefficient (3-D)
C_l	=	section lift coefficient (2-D)
C_M	=	pitching-moment coefficient (3-D)
C_m	=	section pitching-moment coefficient (2-D)
C'	=	numerical coefficient
Ma	=	Mach number
n_D	=	number of devices
S	=	wing surface
S_{ref}	=	wing reference surface
s	=	local coordinate along span
α	=	angle of attack
Γ	=	local circulation
ε	=	angle of horizontal tail plane incidence
η	=	angle of high-lift-device deflection

Subscripts

FW	=	fuselage and wing
H	=	horizontal tail plane
TO	=	takeoff

Presented as Paper 5872 at the 12th AIAA/ISSMO Multidisciplinary Analysis and Optimization Conference, Victoria, British Columbia, Canada, 10–12 September 2008; received 19 December 2008; revision received 30 June 2009; accepted for publication 2 July 2009.

*Research Assistant, Institute of Aircraft Design and Lightweight Structures, Hermann-Blenk-Strasse 35; c.werner-spatz@tu-bs.de. Member AIAA.

†Senior Researcher, Institute of Aircraft Design and Lightweight Structures, Hermann-Blenk-Strasse 35; w.heinze@tu-bs.de.

‡Professor, Head of Institute, Institute of Aircraft Design and Lightweight Structures, Hermann-Blenk-Strasse 35; p.horst@tu-bs.de.

I. Introduction

THE use of high-lift devices on civil transport aircraft has been standard practice at least since the introduction of the swept wing, when they became a necessary means for satisfying field length requirements while allowing the wing and airfoil geometry to be optimized for the high cruise speeds now achievable. A broad range of different device types has been developed over the years, including leading-edge and trailing-edge devices [1] as well as powered high-lift-system concepts [2]. Reference [1] gives an overview of passive high-lift systems and their application on transport aircraft, showing that slats and slotted flaps are the most widely used system combination.

Although the positive effects of slotted flaps have been known for almost a century [3], the underlying physics of the highly complex flows involved were not thoroughly understood until the 1970s, and much of the credit for changing this is given to Smith [4]. It was only after this point that analytical and numerical methods for the design of high-lift devices could be developed. As it was generally accepted that the flow around multi-element airfoils is strongly influenced by boundary-layer and separation effects [5,6], approaches were made by coupling inviscid methods (potential theory or Euler) with integral boundary-layer (IBL) methods, which account for the viscous effects [2,7–10]. Efforts were also concentrated on the development of Reynolds-averaged Navier–Stokes (RANS) solvers capable of correctly predicting flows for high-lift configurations [11–13]. Most of these methods consider only incompressible flow and are restricted to the 2-D case; 3-D results could be derived with so-called quasi-3-D methods, which couple such 2-D methods with a 3-D lifting-surface theory [2,14,15]. Today, 3-D analysis of wing-fuselage-models, including extended high-lift devices with computational fluid dynamics (CFD) methods (Euler and RANS), has become a practicable alternative [16]. However, some topics such as turbulence modeling and transition and separation prediction are still a subject of ongoing research.

Although it is beyond question that the high-lift system must be considered in all stages of aircraft design [5], an accurate prediction of high-lift-system characteristics has not been the top priority for conceptual aircraft design processes. In terms of the overall aircraft, the high-lift-system influences the structural weight and the aerodynamic performance of the aircraft (lift, drag, and pitching moment) during takeoff and landing. Nevertheless, conceptual design processes usually concentrate on designing the aircraft for optimum performance at cruise conditions, a point of view from which the high-lift system can be regarded as a necessary add-on, producing incremental changes in weight and in aerodynamic performance. The influence on structural weight is of minor proportions, as it usually comprises less than 1% of total aircraft weight. As a result, high-lift devices are usually accounted for by using empirical methods. Such

methods are readily available [17–20] and are capable of predicting the characteristics of different types of slat and flap combinations with enough accuracy in terms of both system weight and effects on maximum lift and parasitic drag. Not all methods consider the effects on pitching moment, however, and only some (e.g., [17]) explicitly consider flap effects on induced drag.

This form of high-lift-system representation is bound to become insufficient in the future. It is to be expected that some future transport aircraft designs will focus strongly on short takeoff and landing distances. For these aircraft, the high-lift system will play a far greater role for the overall design than it usually does, and therefore it is desirable to model the characteristics of the high-lift system in greater detail and with more parameter sensitivities than in current processes. Future transport aircraft designs are also likely to consider powered high-lift systems (e.g., systems using air suction or blowing to enhance high-lift performance). Such systems cannot be readily modeled with existing empirical methods, as no database is available, and using a physics-based approach for the representation of such high-lift systems would thus be a necessity. Being the basis for comparison, it would be preferable to model conventional high-lift systems using a physics-based process as well.

Today's state-of-the-art in terms of aerodynamic analysis is the use of CFD methods, especially RANS. However, there are several reasons why CFD methods are not an option for conceptual design processes. The aerodynamic methods cited earlier have been developed for the purpose of designing the high-lift systems themselves. The goals were to develop sufficiently accurate methods to reduce the need for wind-tunnel testing and to provide inverse design capabilities needed for true optimization. Their computational cost is relatively high, even with the computer hardware available today. Compared with wind-tunnel tests, a RANS calculation taking several hours to perform is still an economical alternative, but in a conceptual design process (which requires the consideration of the whole flight envelope and thus hundreds or thousands of calculations for different Mach numbers, angles of attack, and trim conditions), such computation times are prohibitive. Additionally, meshes for 3-D configurations including high-lift devices are very complex and difficult to generate without the need for manual intervention [15,21]. Conceptual design processes usually work iteratively and thus require a high degree of automatization. Finally, CFD models require an exact representation of the complete aircraft surface, including the high-lift system. Geometric data available during the early stages of configuration development often lack the level of detail required for such an analysis.

The next step would be to resort to inviscid/viscous interaction methods using potential theory for the inviscid calculations. However, the computational costs of these methods are still relatively high because they require solution of the boundary-layer equations as well as algorithms for correlating the inviscid and the boundary-layer flow, all in addition to the inviscid flow solution itself. Although an accurate prediction of maximum obtainable lift is surely not possible without considering the boundary layer and flow separation, [4] shows that the principal effects of high-lift devices are due to flows induced by the airfoil elements on each other. It should therefore be possible to model the increments in lift, induced drag, and pitching moment for most of the flight envelope with potential theory alone. Such a method omits viscous effects that lead to flow separations and the limitation of lift, but it offers the advantage of analyzing the complete 3-D configuration at a comparatively low computational cost.

This paper describes a methodology that uses a multiple-lifting-line method as a physics-based approach to compute the aerodynamic characteristics of aircraft in high-lift configurations. Conventional high-lift devices are represented simply by locating singularities at their extended positions. As this method is fully embedded in a multidisciplinary conceptual design process, relevant aspects of the design process itself are presented first. Then the proposed methodology is discussed, showing validation results obtained for two different aircraft and high-lift-system designs. Finally, a quasi-3-D approach is applied to improve predictive accuracy by synthesizing explicit lifting-line and airfoil polar interpolation results. This method, though increasing the computational cost and the required amount of input data, is able to introduce some degree of nonlinear behavior and to improve the prediction of viscous drag, eliminating two major shortcomings of the lifting-line method.

II. Multidisciplinary Conceptual Aircraft Design Process

The design process that serves as a background for the work reported in this paper is the preliminary aircraft design and optimization tool (PRADO), an in-house development of the Institute of Aircraft Design and Lightweight Structures [22]. An overview of the design process structure can be found in Fig. 1. PRADO is a multidisciplinary, integrated, iterative design process. At its core is a set of design modules, each of which performs a specific task in the design process. For example, some modules are responsible for creating the geometry description of individual aircraft components, taking a user-provided parametric description as an input. Other modules are responsible for determining the required engine thrust, for determining the aircraft range and fuel consumption, for determining the aircraft structural weight, etc. Most of these modules require the aerodynamic characteristics of the aircraft for given flight conditions. These are provided by the aerodynamics module, which performs the aerodynamic analysis of the aircraft design, creating a database for use in subsequent modules.

The design modules are based on a common set of program libraries written in FORTRAN. The design process for each aircraft design can be assembled individually from the available modules. Some modules (e.g., winglet geometry) are used only if applicable to the current design. This modularity together with the fact that the modules are task-oriented and not method-oriented makes it possible to implement different versions of each module and then individually select the methodology applied for each design discipline, adapting the balance between computational complexity and result accuracy according to the needs and priorities of the aircraft design being studied. For the prediction of mission fuel consumption, for example, the choices include a simple analysis of the Breguet equation as well as a time-step-based flight simulation. Structural sizing can be performed with choices of methods ranging from classic empirical or semi-empirical methods over simple physics-based methods (bending beam model) up to higher-fidelity finite element methods. Despite its name, PRADO is a tool basically aimed at the conceptual design phase (according to the design phase definitions found in [23]). However, depending on the choice of methods, result detail levels and result accuracy more typical of the preliminary design phase (as defined in [2]) can be obtained.

As can be seen in Fig. 1, all design modules use a common interface (the data management system) to communicate with the aircraft data, which is stored in a set of ASCII-format database files. Initial data are provided by the user and have to include a parametric description of the aircraft layout, the transport mission, and all

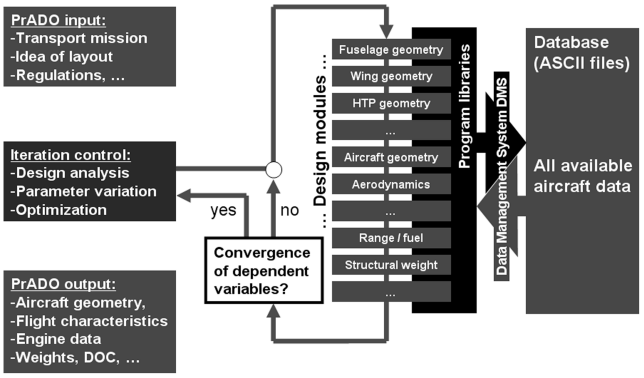

Fig. 1 Overview of the preliminary design process (DOC denotes direct operating cost).

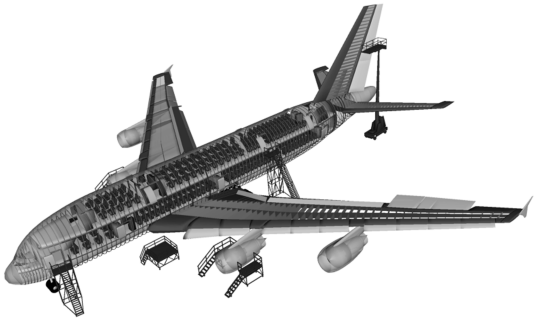

Fig. 2 PRADO geometry model example.

relevant constraints and design targets. Results produced by the design process are available as numerical data in these database files, but many results are also prepared for graphical output using the tool Tecplot® [24]. The PRADO geometry model, as shown in Fig. 2 for a sample aircraft design, contains explicit representations of structural elements, fuel tanks, cabin furnishings and control surfaces, which include the high-lift system.

Apart from the design modules, PRADO features a set of programs that control the iteration of the design process, allowing either an iterative analysis of a single design, an automated parameter variation over one or more user-chosen parameters, or a design optimization with a user-chosen target function and user-chosen design variables. Virtually any parameter available in the database can be selected as a variation parameter, a design variable, or a target function.

For the work presented in this paper, no complete design analysis is performed. Instead, the focus lies on the aerodynamic analysis of conventional transport aircraft using passive high-lift systems. For this reason, the consideration of the aerodynamic characteristics within the design process is to be discussed in more detail.

The discipline of aerodynamics is among the most important in the design process, because many parameters of the design (range, required thrust, structural weight, etc.) are influenced strongly by the aircraft's aerodynamic characteristics. The approach implemented in PRADO uses an aerodynamic database, which provides data (lift, drag, and pitching-moment coefficients for the aircraft) for discrete combinations of altitude, Mach number, angle of attack, and horizontal tail plane (HTP) incidence angle. Data for flight conditions between these discrete combinations are determined through linear interpolation. The database is organized so that the trimmed flight condition can be considered, as shown in Eqs. (1–3):

$$C_L(\alpha, Ma, \varepsilon_H) = C_{L,\mathrm{FW}}(\alpha, Ma) + \Delta C_{L,H}(\alpha, Ma, \varepsilon_H) \quad (1)$$

$$C_D(\alpha, Ma, \varepsilon_H, A) = C_{D0}(Ma, A) + C_{Di,\mathrm{FW}}(\alpha, Ma) + \Delta C_{Di,H}(\alpha, Ma, \varepsilon_H) \quad (2)$$

$$C_M(\alpha, Ma, \varepsilon_H) = C_{M,\mathrm{FW}}(\alpha, Ma) + \Delta C_{M,H}(\alpha, Ma, \varepsilon_H) \quad (3)$$

The aircraft coefficients are composed of base components corresponding to the fuselage and wing and deltas resulting from the presence of the HTP. To calculate these components, several aerodynamic analyses are performed for each combination of Mach number and angle of attack: first, the fuselage and wing alone are computed, and then the complete aircraft (fuselage, wing, and HTP) is analyzed for every angle of HTP incidence. The HTP deltas are determined by subtracting the base components from the coefficients obtained for the aircraft with HTP. This way, it is ensured that the HTP deltas include not only the lift, drag, and pitching-moment of the HTP itself, but also the up- or downwash induced on the wing. For the drag coefficient, zero-lift drag (depending on altitude and Mach number) is considered as an additional component. Using this approach, an aerodynamic database set up with 15 Mach numbers, 20 angles of attack, and 15 HTP incidence angles requires 4800 aerodynamic analyses of the 3-D configuration.

The base coefficients and the HTP deltas are stored in the aircraft database files. Subsequent modules can access the database through a dedicated program library by providing a specific flight situation (described by altitude, Mach number, aircraft configuration, weight, and c.g. position). From these data, required values of lift coefficient and pitching-moment coefficient for trimmed flight can be derived. Using the aerodynamic database, a combination of angle of attack and angle of HTP incidence is determined that satisfies both requirements, providing the total drag (including trim drag) incurred in this flight situation as a result.

Methods available for aerodynamic analysis include a simple handbook method, a multiple-lifting-line method (which is used for the methodology described in this paper), and a panel method [25]. Although these methods provide lift and moment coefficients as well as induced drag, viscous and lift-independent drag is predicted using a handbook method based on Hoerner [26], which uses a flat-plate analogy for viscous drag and includes empirical formulas (e.g., for pressure drag, compressibility, and interference drag).

The aerodynamic database has to be calculated only once for the iteration step, and access to the data is independent of the method chosen for aerodynamic analysis. As long as the geometry of the aircraft does not change during the iteration, the aerodynamic characteristics (which depend solely on the geometry) need only be computed once for the whole design analysis.

The basis for the consideration of a high-lift system is the distinction between four different configurations of an aircraft design: cruise, takeoff, approach, and landing. Each configuration is characterized by a user-provided flap and slat setting (assuming a passive high-lift system consisting of deflectable leading- and trailing-edge devices). The cruise configuration usually features the clean wing with all high-lift devices retracted. The takeoff and approach configurations often use identical flap and slat settings. The aerodynamic database includes aerodynamic data for each of these four configurations. Subsequent modules (especially those that analyze flight cases corresponding to takeoff, approach, or landing) can access this information by choosing the applicable configuration, as described earlier. The question of high-lift-system representation methodology is thus reduced to the task of determining the aerodynamic coefficients for an aircraft with high-lift devices in the extended position.

III. Multiple-Lifting-Line Method

The multiple-lifting-line software LIFTING_LINE was originally developed at the DLR, German Aerospace Center by Horstmann [27]. Although simple lifting-line methods discretize a wing with only one lifting vortex, LIFTING_LINE is able to use several discrete lifting vortices along the wing chord, thereby improving pitching-moment prediction as well as the representation of swept and tapered wings. Unlike a vortex-lattice method, which also has discrete vortices in the chordwise direction but uses a piecewise-constant discretization in the spanwise direction (leading to so-called horseshoe vortices), LIFTING_LINE uses a quadratic approach for the circulation Γ in the spanwise direction (along the coordinate s) on discrete wing segments, according to Eq. (4):

$$\Gamma(s) = A' + B's + C's^2 \quad (4)$$

The discretization both in spanwise and chordwise directions leads to geometry models such as the one shown in Fig. 3. Each lifting surface (wing and HTP here) is divided into a number of elements that, for ease of terminology, will be referred to as panels in this paper, bearing in mind that they are not surface panels. To determine the coefficients A', B', and C', two boundary conditions (continuous circulation and continuous first derivative over panel boundaries) are used together with the kinematic flow condition, which is fulfilled at the middle of the panel in the spanwise direction and at three-quarters of the panel chord. Although not as accurate as lifting-surface methods (which use continuous vorticity both in the

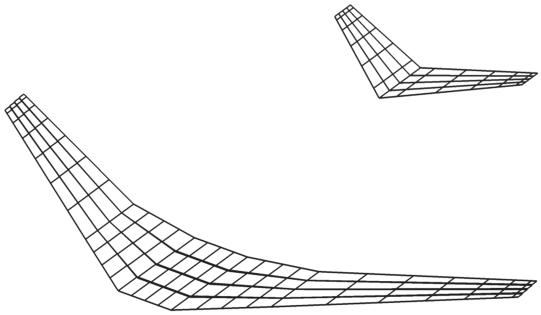

Fig. 3 F11 LIFTING_LINE model.

chordwise and in spanwise directions), LIFTING_LINE has the advantage that it requires a less fine discretization in the spanwise direction than vortex-lattice methods do, on the one hand, but is not as complicated to adapt to different geometries as lifting-surface methods are, on the other hand. The result is a method capable of analyzing single or multiple lifting surfaces that may be swept, tapered, and in nonplanar arrangement.

The aerodynamic analysis is performed by solving the linearized potential equation for thin wings in subsonic flow. Compressibility effects can by accounted for by applying a Göthert correction, as described in [28].

IV. Representation of High-Lift Systems

In this section, after a short overview of the physical effects of deflecting high-lift devices, two methods for representing conventional high-lift devices in conceptual design are discussed. First, the empirical method that has been used in PRADO for years is presented, and then a method that models high-lift devices explicitly is introduced.

Passive high-lift devices mainly rely on at least one of two mechanisms for increasing lift. The first is an increase in camber, an effect that is used by any device that deflects in a rotatory movement. A change in camber displaces the angle of attack required for zero lift, thus producing more lift if a given angle of attack is held constant. The pitching moment also increases, as it is directly proportional to the produced lift. Unlike a flat plate, a cambered wing at zero total lift has areas with upward forces and areas with downward forces. Although the forces compensate each other (producing zero lift as a result), induced drag depends on the square of these forces and is not canceled: a cambered wing at zero lift will still produce induced drag. In addition, the deflected device will also increase parasitic drag, especially the lift-independent pressure drag. The second effect is an increase in effective wing area, which is used by devices that extend through translatory movements. An increased wing area at a constant angle of attack will generate more lift. Because the wing reference area used in the aerodynamic coefficient definition is usually left constant, the additional lift translates into an increased lift coefficient. In this case, the pitching moment will increase more than the lift force if the reference point remains unchanged, because not only the lift force itself increases, but also its effective position changes if the section chord is increased. Viscous drag is also increased because the flow has to pass over a bigger surface. Methods used for the representation of high-lift devices in an aircraft design process can be judged by their ability to account for these effects. A third effect used especially by slotted high-lift devices (namely, influencing the boundary layer to delay flow separation) is not modeled by the methods discussed in this section and is only named here for completeness.

The empirical method for high-lift-system representation is based on statistical results for the effects of different high-lift-system types. In this case, the method is based on values proposed by Roskam (taken from [19]). According to this method, the high-lift system consists of two components: leading-edge devices and trailing-edge devices. A template file contains statistical values for the effects that different leading- and trailing-edge device types have on the airfoil-section lift, zero-lift drag, and pitching-moment coefficients at the maximum device deflection angle $\eta_{\max}$. These values are shown in Table 1. For a given aircraft configuration [e.g., takeoff (TO)] with a given device deflection angle h_{TO}, the coefficient increments are interpolated according to Eq. (5):

$$\Delta C_{l,\mathrm{TO}} = \Delta C_l(\eta_{\max}) \cdot \frac{\eta_{\mathrm{TO}}}{\eta_{\max}} \tag{5}$$

As shown in Eq. (6), the 3-D coefficients are computed by relating the area of the wing segment to which the device is attached (S_i) to the wing reference area S_{ref}. At the same time, the influence of the sweep angle is considered using the quarter-chord-line sweep of the wing segment $\varphi_{25,i}$. The increments for all n_D devices on the wing are then added up.

$$\Delta C_{L,\mathrm{TO}} = \frac{1}{S_{\mathrm{ref}}} \cdot \sum_{i=1}^{n_D} \Delta C_{l,\mathrm{TO},i} \cdot S_i \cdot \cos(\varphi_{25,i}) \tag{6}$$

The same procedure is applied to the drag and pitching-moment increments as well as to the increments for the approach and landing configurations. When building the aerodynamic database, aerodynamic analyses are performed for the clean aircraft geometry, as described in Sec. II. At every combination of Mach number and angle of attack, the base coefficients for the fuselage and wing are used together with the empirical increments to produce the base coefficients of the high-lift configurations, as shown exemplarily for the takeoff configuration in Eqs. (7–9). The increments themselves are considered to be independent of altitude, Mach number, and angle of attack. The increment of the drag coefficient is taken to be an increment in parasitic drag. The increase in induced drag caused by increasing camber is thus not explicitly captured by this approach:

$$C_{L,\mathrm{FW,TO}}(\alpha, Ma) = C_{L,\mathrm{FW}}(\alpha, Ma) + \Delta C_{L,\mathrm{TO}} \tag{7}$$

$$C_{D0,\mathrm{FW,TO}}(Ma, A) = C_{D0}(Ma, A) + \Delta C_{D0,\mathrm{TO}} \tag{8}$$

$$C_{M,\mathrm{FW,TO}}(\alpha, Ma) = C_{M,\mathrm{FW}}(\alpha, Ma) + \Delta C_{M,\mathrm{TO}} \tag{9}$$

Table 1 Empirical values for high-lift-system performance prediction (based on [19], part 6, p. 360)

Device type	Location	Max deflection angle, deg	Airfoil coeff C_l	Deltas at max C_{d0}	Deflection C_m
Krueger flap	Leading edge	80	0.50	0.00	−0.10
Slat	Leading edge	30	0.93	0.00	0.11
Hinged nose	Leading edge	30	0.80	0.00	−0.09
Split flap	Trailing edge	60	0.80	0.23	−0.28
Plain flap	Trailing edge	60	0.90	0.12	−0.28
Fowler flap	Trailing edge	30	1.67	0.10	−0.42
Single-slotted flap	Trailing edge	40	1.18	0.13	−0.33
Double-slotted flap	Trailing edge	55	1.40	0.23	−0.41
Triple-slotted flap	Trailing edge	55	1.60	0.23	−0.44
Double fowler flap	Trailing edge	30	2.25	0.15	−0.44

In subsequent modules, these base coefficients are used together with the increments for HTP incidence when computing trimmed flight conditions for the takeoff, approach, or landing configurations.

The main advantage of this method is that only the clean aircraft configuration needs to be explicitly analyzed. When using LIFTING_LINE, a relatively coarse discretization is usually enough to obtain sufficiently accurate results (approximately 4 panels in the chordwise direction and 10 in the spanwise direction). With such models, a single computation (with 20 angles of attack) takes only 2–3 s on a standard personal computer. The complete aerodynamic database for the aircraft can be generated in approximately 15 min.

The disadvantages of this method include the fact that the effects of high lift, as discussed earlier, are not treated separately and it is not possible to determine to which extent each physical effect is accounted for in the empirical increments. Changes in lift-curve slope due to increased camber cannot be predicted by this method. Furthermore, the validity of the increments must be questioned with every new design, as the database from which they are compiled is limited. Also, high-lift devices of the same type are always treated in the same manner, with only little consideration of individual flap geometry (e.g., flap chord is not considered). Finally, linear scaling for the deflection angle is not guaranteed to produce realistic results in all cases.

An attempt to overcome some of these limitations is made by explicitly modeling the geometry of the high-lift devices for each of the four configurations (cruise, takeoff, approach, and landing). For this, the automated model generator that derives the panel model from the PRADO geometry description is enhanced to consider not only the basic wing geometry, but also the geometry of slats and flaps. This has far-reaching consequences on the topology of the model. New panel boundaries have to be introduced at the edges of slats and flaps, both in the spanwise and in chordwise directions. Each panel in the model now corresponds either to the fixed part of the wing geometry or to a high-lift device. Panels belonging to the high-lift devices are positioned according to the slat and flap positions of each configuration, which requires the user to provide accurate descriptions of the high-lift devices' translatory and rotatory extension paths as additional inputs. The result is a different panel model for each high-lift configuration. Panels are positioned in such a way that their quarter-chord line (where the lifting vortex lies) coincides with the chord line of the wing, slat, or flap. Angles of device deflection are considered by adjusting the kinematic flow condition for the corresponding panels. It is apparent that the models for the explicit method need to have more chordwise panels than those used for the empirical method to ensure a sufficiently accurate discretization of the high-lift device geometry in the deflected positions. An increase in the number of spanwise panels is also necessary, both to sufficiently resolve the local effects at the boundaries of high-lift devices and to provide an adequate relation between panel chordwise and spanwise dimensions.

When building the aerodynamic database with the explicit method, analyses are performed for all combinations of Mach number, angle of attack, HTP incidence, and aircraft configuration. Equations (1–3) have to be extended in the manner shown in Eqs. (10–12), with *i*config denoting the configuration:

$$C_{L,i\text{config}} = C_{L,\text{FW},i\text{config}} + \Delta C_{L,H,i\text{config}} \tag{10}$$

$$C_{D,i\text{config}} = C_{D0,i\text{config}} + C_{Di,\text{FW},i\text{config}} + \Delta C_{Di,H,i\text{config}} \tag{11}$$

$$C_{M,i\text{config}} = C_{M,\text{FW},i\text{config}} + \Delta C_{M,H,i\text{config}} \tag{12}$$

The increase in parasitic drag cannot be modeled by the lifting-line method. Instead, the drag increment values from Table 1 are used. In contrast to the empirical method, however, high-lift device effects on induced drag are also accounted for. Additionally, the coefficient deltas for HTP incidence are different for each configuration, taking into account the changes in induced upwash or downwash caused by the high-lift devices.

The explicit method requires significantly more computation time than the empirical method. First, computational costs increase due to the fact that now each high-lift configuration has to be calculated with the lifting-line method, whereas the empirical method requires only the cruise configuration to be considered. Second, the necessary increase in the number of panels causes the time needed for each calculation to increase. Depending on the panel mesh density, calculation times range from a few seconds to several minutes. Models with approximately 8 panels in the chordwise and 40 panels in the spanwise directions were found to provide accurate results for the configurations studied, while requiring the moderate amount of approximately 90 s per computation (including 20 angles of attack). This would increase the time required to produce a full aerodynamic database to approximately 8 to 10 h. But the database for the high-lift configurations only has to span about half of the Mach number range of the cruise configuration, which allows a reduction of the number of calculations performed. In addition, configurations with the same high-lift device extension angles (such as the takeoff and approach configurations in many cases) only have to be computed once. Taking advantage of this, the time required to build the full database can be reduced to approximately 5–6 h. Although this seems prohibitive in comparison with the computation times of the empirical method, it still allows a full design analysis to be performed in approximately 12 h, which is deemed acceptable for conceptual design studies. The advantages of this method are that results are bound to be more accurate, and more parameter sensitivities are included in the physical model.

V. Application Examples and Results

Results of both methods are shown and compared for two aircraft designs that have been selected based on the availability of wind-tunnel or CFD results for the aerodynamic characteristics. Because these aircraft designs are academic configurations designed for the purpose of performing detailed aerodynamic studies, not all data necessary to perform a complete design analysis are available. Additionally, the focus of this paper is not to demonstrate the complete design process but to validate the presented method for high-lift-system analysis. Therefore, only those modules of the design process needed to produce a geometry model and perform the aerodynamic analysis are used. Also, no full aerodynamic database is computed. Instead, selected parameter combinations are chosen for each configuration based on the wind-tunnel or CFD data available for comparison.

The first aircraft design is derived from the DLR research design dubbed DLR-F11, for which wind-tunnel results of the cruise and the high-lift configurations are available as a comparison baseline [29]. The high-lift-system design and wind-tunnel measurements were performed as part of the Three-Surface-Aircraft project [30]. Figure 4 shows the aerodynamic surface of the PRADO geometry model for this aircraft design. Detailed information of the slat and fowler flap geometries for the wind-tunnel model in its deflected positions is available, and the PRADO model of this geometry can also be seen in Fig. 4. A more detailed depiction of the high-lift system at the wing tip in cruise (retracted), takeoff, and landing configurations is shown in Fig. 5. The takeoff configuration features deflection angles of

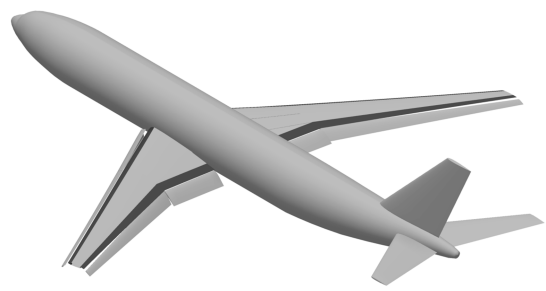

Fig. 4 F11 PRADO surface model with high-lift system in landing configuration.

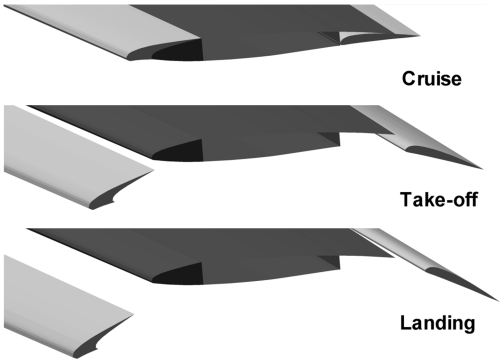

Fig. 5 F11 high-lift device geometry (wing tip, PRADO model).

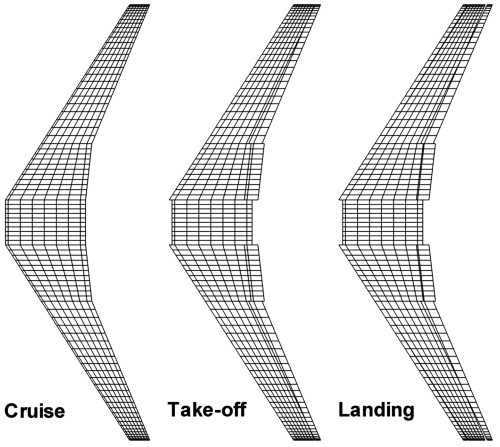

Fig. 6 F11 LIFTING_LINE model (explicit method; wing only).

20 deg for slats and 22 deg for flaps; for the landing configuration, the deflection angles are 26.5 and 32 deg, respectively.

The F11 panel model used for the empirical method (cruise configuration only) is shown in Fig. 3. Figure 6 shows the resulting F11 panel model of the wing used for the explicit method. The cruise, takeoff, and landing configurations are shown. As can be seen, the geometry of all three models is identical for those panels corresponding to the fixed wing, and only the panels representing the slats and flaps change. A comparison between the PRADO geometry model and the resulting panel models can be seen in Fig. 7. Note that all panels in the lifting-line model are always considered to be horizontal. Angles of incidence (as a result, for example, of flap deflection) are considered numerically, as described in Sec. III. However, this adjustment is not visible in the model geometry, explaining the differences in the slat and flap geometry representation seen in Fig. 7.

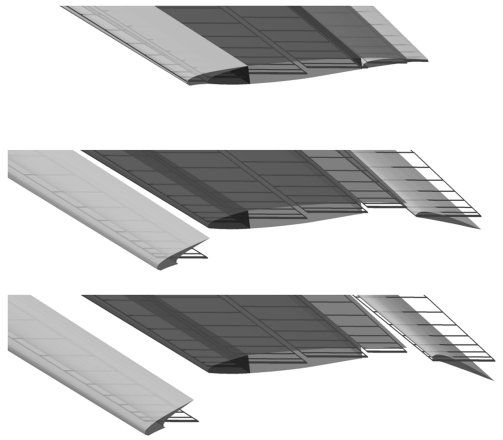

Fig. 7 F11 high-lift device geometry (PRADO/LIFTING_LINE model comparison).

The second aircraft design is a wing-fuselage configuration with a large hinged flap. This design (called FNG for the airfoil it uses: Flugzeug Neuer Generation) has been provided by the Institute of Fluid Mechanics (ISM) of the Technische Universitaet Braunschweig [31]. The single trapezoid wing is arranged in a high-wing configuration. The aircraft design has been selected because of its rather unusual hinged high-lift flap and because results from a 3-D-RANS analysis are available for comparison purposes. Figure 8 shows the aerodynamic surface of the PRADO geometry model for the FNG aircraft. Note that the large fairing on the center fuselage has not been optimized for this configuration. However, this fairing is not explicitly considered in the aerodynamic analysis. As can be seen in Fig. 9, which shows the geometry used for the RANS analysis, the fairing actually considered is significantly smaller. Figure 8 also shows the PRADO model of the hinged flap in its fully extended position. The flap deflection angle is 20 deg for the takeoff configuration and 40 deg for the landing configuration.

The panel model with explicit flap representation for the FNG design is shown in Fig. 10 in the cruise, takeoff, and landing configurations. In this model, two panels are used to model the flap in the chordwise direction. This results from an algorithm that attempts to distribute the total number of panels as evenly as possible between the different chordwise sections, with the limit between sections (the flap hinge line) being at a fixed position. Figure 11 shows this by comparing the PRADO geometry of the large FNG flap (landing position) with lifting-line models featuring different numbers of panels.

Results obtained for the F11 design are shown in Fig. 12, in which data obtained with both the empirical and the explicit methods are compared with wind-tunnel data. Results are given in the form of lift coefficient, pitching-moment coefficient, and total drag coefficient (including zero-lift drag) vs angle of attack. Note that only one flight case is depicted ($Ma = 0.2$ at sea level; HTP at 0 deg incidence). For the cruise configuration, all coefficients predicted by the lifting-line method match the measured coefficients almost exactly in the area of linear lift behavior. This proves that for the case with all high-lift devices retracted, the coarse panel mesh used for the empirical method is sufficient and that the results are independent of mesh density. Of course, the separation-induced nonlinear behavior visible at angles of attack beyond 8 deg cannot be predicted by the linearized potential theory of LIFTING_LINE. For the takeoff and landing configurations, the wind-tunnel results show that there is no longer

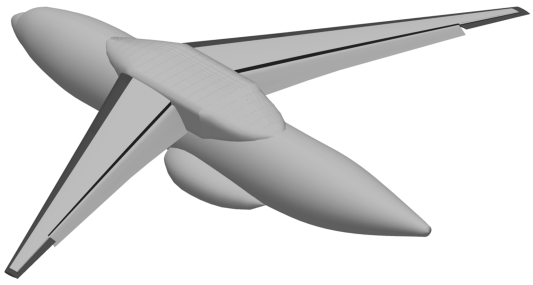

Fig. 8 FNG PRADO surface model with high-lift system in landing configuration.

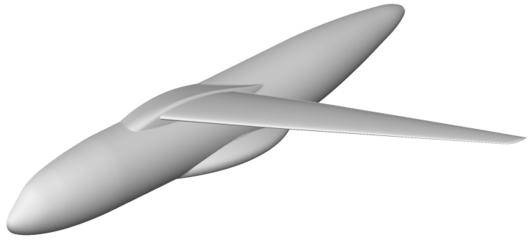

Fig. 9 FNG RANS surface model (provided by ISM).

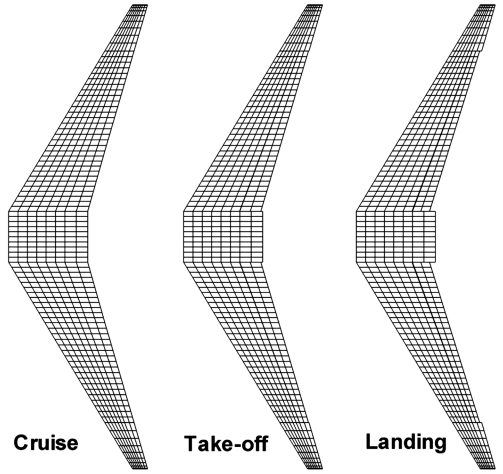

Fig. 10 FNG LIFTING_LINE model (explicit method).

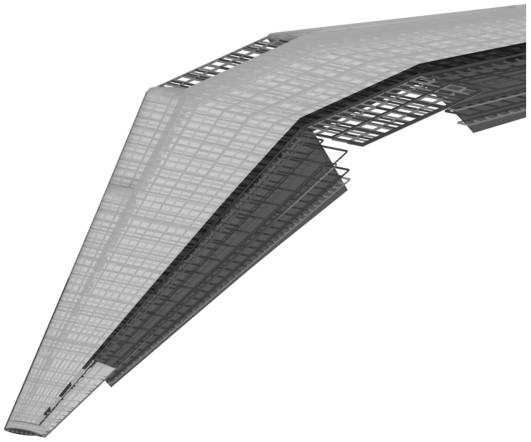

Fig. 11 FNG high-lift device geometry (PRADO/LIFTING_LINE model comparison).

any distinctive linear area. Both the empirical and the explicit methods have to predict linear behavior, however. The empirical method tends to overestimate the lift and moment coefficients over most of the angle-of-attack range, whereas the explicit method underestimates them. In the case of drag, both methods deliver almost the same coefficients, overestimating the drag measured in the wind tunnel. As described in Sec. IV, the explicit method still uses the statistical values for the estimation of zero-lift drag increase due to slats and flaps.

When considering an angle-of-attack range from 5 to 15 deg, the results of the empirical method seem to provide the better approximation for the wind-tunnel results. However, when considering the full range from −5 to 20 deg for the high-lift configurations, the results of the explicit method tend to constitute the better approximation. The main parameter for judging the applicability of both methods to a conceptual design process is their ability to predict coefficient increments. For this, Table 2 shows the average coefficient increments predicted by both methods compared with those measured in the wind tunnel. Because useful results can only be expected in the angle-of-attack range in which lift behavior is mostly linear, the average values are computed only between angles of 0 and 8 deg. In terms of lift and moment coefficients, the absolute deviation of the explicit method is larger in this range. Both methods lie within the 10–20% tolerance cited in [2], as appropriate for conceptual design methods. This is not the case for the drag coefficient, in which both methods agree closely but show a substantial overestimation of total drag.

In summary, for the F11 design both the empirical and the explicit methods for high-lift-system representation produce useful results for a conceptual design process. The statistical coefficient deltas of the empirical method seem well calibrated for this type of high-lift system on this type of aircraft. The explicit method would have the advantage of providing physics-based parameter sensitivities in the event that variations (e.g., in the high-lift-system geometry) were to be studied. However, for the analysis of the given design, the empirical method has the advantage of significantly lower computational cost.

Figure 13 shows the results generated by both methods for the FNG design in comparison with results of a 3-D-RANS analysis. The data are presented in the same manner as in Fig. 12. Again, only one

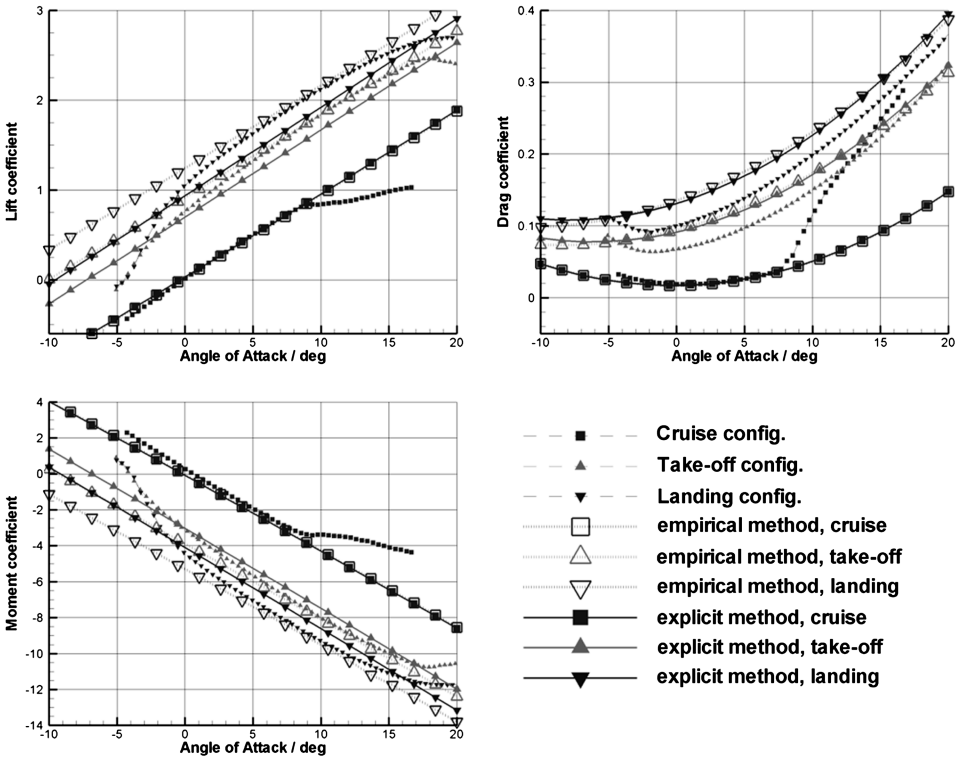

Fig. 12 F11 results (empirical and explicit methods): $Ma = 0.2$; HTP undeflected.

Table 2 Average coefficient increments for the F11 design (AOA range of 0–8 deg)

	Wind tunnel	Empirical method		Explicit method	
Coefficient	ΔC_i	ΔC_i	Error	ΔC_i	Error
Takeoff					
Lift	0.8121	0.8934	10.01%	0.6880	−15.28%
Drag	0.0665	0.0969	45.65%	0.0928	39.55%
Moment	−3.6723	−3.8431	4.65%	−3.0453	−17.07%
Landing					
Lift	1.1149	1.2183	9.28%	0.9423	−16.51%
Drag	0.1061	0.1445	36.25%	0.1616	30.97%
Moment	−5.0604	−5.2427	3.60%	−3.6629	−18.31%

flight case is considered ($Ma = 0.21$ at sea level; wing and fuselage only). As for the F11 design, the predictions for the cruise configuration show good agreement with the RANS results in the area of linear lift behavior, which goes up to an angle of attack of about 13 deg for the FNG. For the high-lift configurations, however, the results of the empirical method are unsatisfactory. Lift, drag, and pitching-moment coefficients are strongly underestimated. Additionally, because the values are scaled linearly with the deflection angle, the delta predicted for the landing configuration is always twice that predicted for the takeoff configuration (40 and 20 deg flap deflections, respectively), even though the RANS results show that the effect of deflecting the flap from 20 to 40 deg has a magnitude different from the effect of deflecting the flap from 0 to 20 deg. Apart from this, the RANS results show a notable reduction in lift-curve slope for the high-lift configurations, which is not predicted by the empirical method. For the explicit method, the results for the high-lift configurations show significant improvement. For the lift and pitching-moment coefficients, the values for the takeoff configuration are somewhat underestimated, whereas the results for the landing configuration are slightly overestimated. However, in contrast to the empirical method, doubling the angle of flap deflection does not double the delta value added to the coefficients. The lift curves for both configurations exhibit a slight decrease in slope in comparison with the lift curve for the cruise configuration. Although this decrease is not as high as is to be expected when comparing with the RANS results, it has to be noted that the RANS models tend to exhibit separated flow over much of the flap chord for all angles of attack studied (cf. [31]), indicating that the RANS curves depicted in Fig. 13 represent a nonlinear behavior and should have a lower slope than any potential theory results. The results obtained for the drag coefficient also improve significantly with the explicit method, although drag coefficient values are still underestimated for all configurations. The deviation for the cruise configuration is most probably due to an underestimation of the zero-lift drag of the fuselage and wing. For the takeoff and landing configurations, the additional zero-lift drag of the flap and the interference drag at the spanwise edges of the large flap are also underestimated, causing the gap between PRADO and RANS results to increase with flap deflection.

In the limited angle-of-attack range available in the RANS data, the attempt is made again to judge both methods on their ability to predict coefficient increments over the cruise configuration due to flap deflections. The increments are averaged over an angle-of-attack (AOA) range from 6 to 11 deg and are shown in Table 3. As expected, the increments obtained with the empirical method are not acceptable even for the conceptual design stage. It seems that the statistical values used are not applicable to this high-lift configuration with its rather unusually large plain flap. For the explicit method, the predicted increments show errors mostly lower than 20% and are thus acceptable for conceptual design. Higher deviations are obtained for the lift and pitching-moment coefficients of the landing configuration, although this is most probably caused by the fact that the available RANS data lie completely in the area of nonlinear behavior.

Overall results for the FNG design show clearly that for rather unusual aircraft and/or high-lift-system layouts, the explicit method can produce far better results than the empirical method, thus justifying the significant increase in computation time. When using the explicit method for the generation of a complete aerodynamic database, the process architecture can be optimized beyond the measures described in Sec. IV to reduce the computation time penalty. As both aircraft designs studied here have shown, the cruise configuration (for which the database has to cover a large Mach number and altitude range) can be analyzed with the coarse panel mesh used for the empirical method without any detrimental influence on the results. The finer panel model only needs to be used for the high-lift configurations (takeoff, approach, and landing).

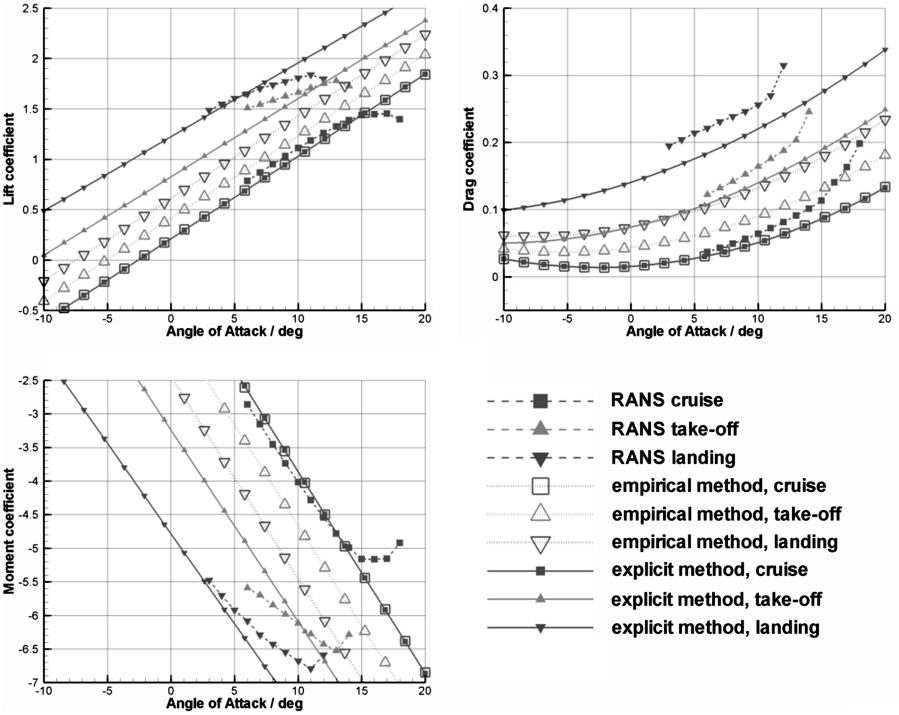

Fig. 13 FNG results (empirical and explicit methods): $Ma = 0.21$; wing and fuselage.

Table 3 Average coefficient increments for the FNG design (AOA range of 6–11 deg)

	RANS	Empirical method		Explicit method		POLINT	
Coefficient	ΔC_i	ΔC_i	Error	ΔC_i	Error	ΔC_i	Error
Takeoff							
Lift	0.6148	0.1975	−67.87%	0.5803	−5.61%	0.5338	−13.17%
Drag	0.0944	0.0370	−60.75%	0.0836	−11.46%	0.0910	−3.59%
Moment	−2.3344	−0.7915	−66.09%	−2.2650	−2.98%	−2.1286	−8.82%
Landing							
Lift	0.7615	0.3950	−48.12%	0.9423	23.74%	0.7363	−3.31%
Drag	0.1899	0.0768	−59.55%	0.1616	−14.87%	0.1866	−1.70%
Moment	−2.8856	−1.5831	−45.14%	−3.6629	26.94%	−2.8326	−1.84%

VI. Polar Interpolation Method

As discussed in Sec. III, the multiple-lifting-line method used for the aerodynamic analysis uses a linearized potential theory formulation for thin airfoils and thus has some limitations, as can been seen in the results presented so far. Because no boundary layer is considered, no prediction of viscous drag can be made. Instead, only induced drag is predicted by LIFTING_LINE, leading to an offset from the total drag from wind-tunnel measurements and RANS analyses, which so far has been closed by applying a handbook method based on Hoerner [26] (cf. Sec. II). Another limitation of the lifting-line method is that it only produces a linear dependency between lift and angle of attack. Nonlinear behavior, which is a result of beginning separation and thus related to the behavior of the boundary layer, is not predicted.

An alternate method for drag prediction is based on the assumption that if the total drag of different airfoil sections of a wing is known, the total lift-independent drag of the wing can be derived by interpolating between the airfoil drag values. This interpolation is performed by the program POLINT [32], which is embedded in PRADO's aerodynamics module as an additional option to be used together with the explicit method. The approach is comparable with the quasi-3-D methods cited in Sec. I, although in this case, the generation of the airfoil-section data is not part of the process. Instead, the user has to provide the airfoil polars, which may originate from in-flight measurements, wind-tunnel measurements, or higher-order CFD computations, for example. It is assumed that the airfoil polars include viscous effects and are therefore defined by Mach number, Reynolds number, and the airfoil geometry for which they were generated. If a wing features variable airfoil-section geometry along its span, polars for different airfoils at arbitrary spanwise positions can be provided. The function of POLINT is shown in Fig. 14. POLINT is used as a postprocessor for LIFTING_LINE results. A loop is performed over all cuts, and each cut corresponds to one chordwise row of panels in the LIFTING_LINE model. For each cut, an airfoil polar is interpolated from the surrounding available polars in terms of Mach number, Reynolds number, and spanwise position. The current Reynolds number is based on freestream velocity, local chord, and altitude (for the high-lift configurations, sea level is assumed). The local lift coefficient for the streamwise cut is then taken from the LIFTING_LINE results, and the angle of attack corresponding to this lift coefficient in the airfoil polar is determined. The lift coefficient is reduced if it lies beyond the maximum lift coefficient of the polar. Then, based on the angle of attack determined, the corresponding drag and pitching-moment coefficients are retrieved from the airfoil polar. At the end of the loop, these coefficients form the new spanwise distributions and determine the 3-D coefficients, which are written back to the PRADO database instead of the original LIFTING_LINE results. In the case of drag, the drag coefficient from LIFTING_LINE (induced drag only) is added to the profile drag determined by POLINT.

It is to be noted that POLINT does not explicitly consider influences of sweep angle and assumes that all airfoil polars are given

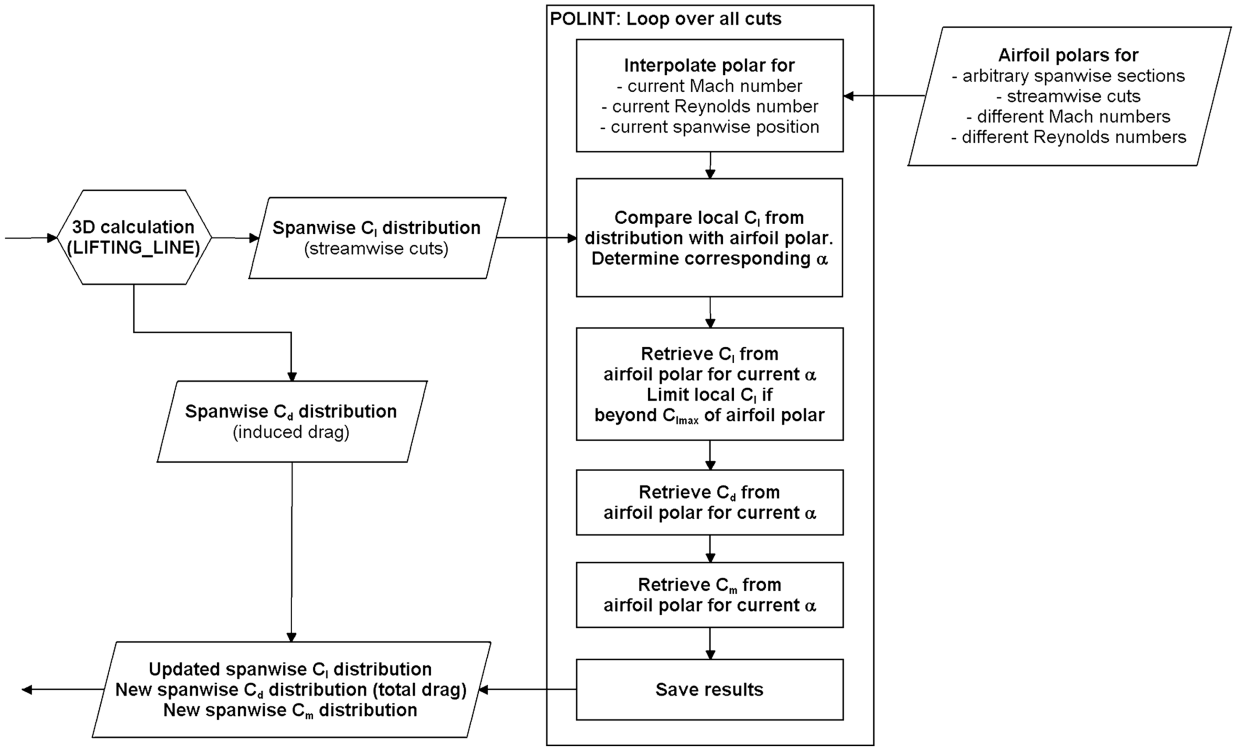

Fig. 14 POLINT structure.

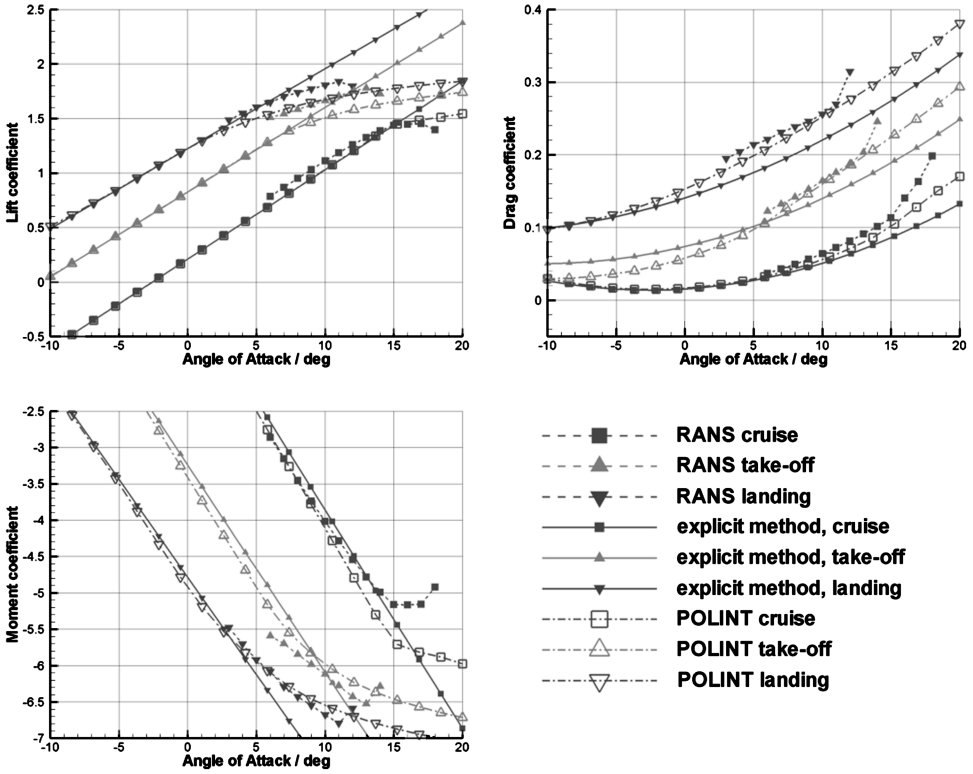

Fig. 15 FNG results (explicit method and POLINT): $Ma = 0.21$; wing and fuselage.

for streamwise cuts (where streamwise means parallel to the undisturbed flow). If a swept wing is to be analyzed, the airfoil polars have to be transformed beforehand. For tapered wings, using the sweep angle of the quarter-chord line is recommended [33]. At the same time, it has to be considered that the fuselage intersection and the wingtip have no aerodynamically effective sweep. It becomes apparent that the choice of the spanwise positions at which airfoil polars are considered influences the results. At least four positions are required for a single trapezoid planform: the fuselage intersection (or symmetry plane if no fuselage is present) with zero sweep angle, the wingtip with zero sweep angle, and two intermediate positions with an effective sweep angle corresponding to the quarter-chord sweep of the trapezoid. Between the fuselage intersection and the first intermediate position, as well as between the second intermediate position and the wingtip, the influence of the sweep angle increases and decreases linearly as a result of the linear polar interpolation.

Of the two aircraft designs studied, the polar interpolation method can only be applied to the FNG, due to the availability of airfoil polars generated through 2-D RANS analysis. Figure 15 shows the results obtained compared with the RANS results and the results of the explicit method. At a first glance, the resulting total drag coefficients seem to improve most of all, compared with the results presented in Fig. 13. The values predicted now closely match those resulting from RANS analysis, leaving only a very small gap. For the lift coefficient, the values for the cruise configuration improve in the area of maximum lift as the nonlinear form of the curve is now approximated by the POLINT results. It becomes obvious, however, that a precise prediction of the maximum lift coefficient is not possible with this method. The reason for this is that the maximum lift generated by a three-dimensional swept wing depends largely on factors such as separation that is transported by the crossflow along the span. Such three-dimensional effects cannot be accounted for by the polar interpolation method, the result being that the nonlinear lift curve moves toward a maximum value with increasing angle of attack, for which further studies may show a possibility to derive an estimate of the aircraft maximum lift coefficient. For the high-lift configurations, the increments obtained in the AOA range from 6 to 11 deg are listed in Table 3. It becomes evident that for the takeoff configuration, the deviations of the lift and pitching-moment coefficients increase. Despite the underestimation of the coefficients, however, the lift-curve slope matches the RANS results more closely than with the explicit method alone. For the landing configuration, lift and pitching-moment coefficient increments are predicted more accurately with POLINT, as is the lift-curve slope and the gap between the lift curves of the takeoff and landing configurations. Overall, result quality can be described as very good for the conceptual design stage. In particular, drag coefficients can be predicted with an accuracy difficult to achieve using other methods.

VII. Conclusions

Explicit high-lift device representation and polar interpolation are methods that improve the fidelity of predicted high-lift-system aerodynamic characteristics in the aircraft conceptual design stage. Although the explicit modeling method is capable of predicting the aerodynamic coefficient increments for slat and flap arrangements with good accuracy, the polar interpolation method improves drag prediction and provides some degree of nonlinear aerodynamic behavior, possibly aiding in the estimation of the maximum lift coefficient.

The results of these methods are superior to those obtained with empirical methods, because empirical methods produce accurate results only for aircraft designs and high-lift device types for which they are properly calibrated, whereas the explicit modeling and polar interpolation can be applied to virtually any design. However, these methods require more data and also increase the computational cost: for the explicit modeling, the high-lift-system geometry has to be provided in some detail, and for the polar interpolation method, airfoil polars have to be available beforehand.

Nevertheless, at least for aircraft designs for which the performance of the high-lift system plays a determining role (e.g., aircraft with innate short takeoff and landing capabilities), these two methods still represent good solutions for the conceptual design stage, as their modeling effort and computational cost are still far below those necessary for other methods that would provide similar or better results, such as CFD analysis of the whole three-dimensional configuration.

In theory, the polar interpolation method provides the means to consider any form of high-lift system, as long as corresponding

airfoil polars are available. With further development of the process, the prediction of aerodynamic characteristics of aircraft designs using powered high-lift systems (i.e., blowing or suction) will become possible in the future.

Acknowledgments

The authors wish to thank the Institute of Aerodynamics and Flow Technology at the DLR, German Aerospace Center for providing the LIFTING_LINE code, the POLINT code, and the F11 configuration data and wind-tunnel results. The authors also wish to thank the Institute of Fluid Mechanics of the Technische Universitaet Braunschweig for providing the "Flugzeug Neuer Generation" configuration data and Reynolds-averaged Navier–Stokes results.

References

[1] Rudolph, P. K. C., "High-Lift Systems on Commercial Subsonic Airliners," NASA CR-4746, 1996.

[2] Dillner, B., May, F. W., and McMasters, J. H., "Aerodynamic Issues in the Design of High-Lift Systems for Transport Aircraft," *Improvement of Aerodynamic Performance Through Boundary Layer Control and High Lift Systems*, AGARD CP-365, Neuilly-sur-Seine, France, 1984.

[3] Woodward, D. S., and Lean, D. E., "Where is High-Lift Today?—A Review of Past UK Research Programmes," *High-Lift System Aerodynamics*, AGARD CP-515, Neuilly-sur-Seine, France, 1993.

[4] Smith, A. M. O., "High-Lift Aerodynamics," *Journal of Aircraft*, Vol. 12, No. 6, 1975, pp. 501–530. doi:10.2514/3.59830

[5] Butter, D. J., "Recent Progress on Development and Understanding of High Lift Systems," *Improvement of Aerodynamic Performance Through Boundary Layer Control and High Lift Systems*, AGARD CP-365, Neuilly-sur-Seine, France, 1984.

[6] Meredith, P. T., "Viscous Phenomena Affecting High-Lift Systems and Suggestions for Future CFD Development," *High-Lift System Aerodynamics*, AGARD CP-515, Neuilly-sur-Seine, France, 1993.

[7] Drela, M., and Giles, M. B., "Viscous-Inviscid Analysis of Transonic and Low Reynolds Number Airfoils," *AIAA Journal*, Vol. 25, No. 10, 1987, pp. 1347–1355. doi:10.2514/3.9789

[8] Kusunose, K., Wigton, L. B., and Meredith, P. T., "A Rapidly Converging Viscous/Inviscid Coupling Code for Multi-Element Airfoil Configurations," AIAA Paper 91-0177, 1991.

[9] Mathews, J. R., "The Aero-Mechanical Design of a Novel Fowler Flap Mechanism," *High-Lift System Aerodynamics*, AGARD CP-515, Neuilly-sur-Seine, France, 1993.

[10] Verhoff, A., Michal, T., and Cebeci, T., "A Viscous Interaction Approach for Analysis and Design of Airfoils and High-Lift Configurations," AIAA Paper 97-0510, 1997.

[11] Fritz, W., "Maximum, and High-Lift Characteristics of Multi-Element Airfoils," *High-Lift System Aerodynamics*, AGARD CP-515, Neuilly-sur-Seine, France, 1993.

[12] Rogers, S. E., Wiltberger, N. L., and Kwak, D., "Efficient Simulation of Incompressible Viscous Flow over Multi-Element Airfoils," *High-Lift System Aerodynamics*, AGARD CP-515, Neuilly-sur-Seine, France, 1993.

[13] Rudnik, R., Melber, S., Ronzheimer, A., and Brodersen, O., "Three-Dimensional Navier-Stokes Simulations for Transport Aircraft High-Lift Configurations," *Journal of Aircraft*, Vol. 38, No. 5, 2001, pp. 895–903. doi:10.2514/2.2849

[14] Jacob, K., "A Fast Computing Method for the Flow over High-Lift Wings," *High-Lift System Aerodynamics*, AGARD CP-515, Neuilly-sur-Seine, France, 1993.

[15] Reckzeh, D., "Rechenverfahren für den Entwurfsprozess von Hochauftriebskonfigurationen," *DGLR Jahrbuch 1998, Band 2*, DDeutsche Gesellschaft für Luft- und Raumfarht, Bonn, Germany, 1998.

[16] Perraud, J., Cliquet, J., Houdeville, R., Arnal, D., and Moens, F., "Transport Aircraft Three-Dimensional High-Lift Wing Numerical Transition Prediction," *Journal of Aircraft*, Vol. 45, No. 5, 2008, pp. 1554–1563. doi:10.2514/1.32529

[17] Raymer, D. P., *Aircraft Design: A Conceptual Approach*, AIAA Education Series, AIAA, Reston, VA, 2006.

[18] Torenbeek, E., *Synthesis of Subsonic Airplane Design*, Delft Univ., Delft, The Netherlands, 1982.

[19] Roskam, J., *Airplane Design*, Vols. 1–8, Roskam Aviation and Engineering Corp., Ottawa, KS, 1985.

[20] Howe, D., *Aircraft Conceptual Design Synthesis*, Professional Engineering Publishing, Suffolk, England, U.K., 2000.

[21] Flaig, A., and Hilbig, R., "High-Lift Design for Large Civil Aircraft," *High-Lift System Aerodynamics*, AGARD CP-515, Neuilly-sur-Seine, France, 1993.

[22] Heinze, W., "Ein Beitrag zur Quantitativen Analyse der Technischen und Wirtschaftlichen Auslegungsgrenzen Verschiedener Flugzeugkonzepte für den Transport Grosser Nutzlasten," Technische Univ. Braunschweig, Zentrum für Luft- und Raumfahrt, Rept. 94-01, Braunschweig, Germany, 1994.

[23] Nicolai, L. M., *Fundamentals of Aircraft Design*, METS, Inc., San Jose, CA, 1975.

[24] Tecplot, Software Package, Ver. 10.0, Amtech Engineering, Inc., Bellevue, WA, 2003.

[25] Österheld, C. M., "Physikalisch Begründete Analyseverfahren im Integrierten Multidisziplinären Flugzeugvorentwurf," Technische Univ. Braunschweig, Zentrum für Luft- und Raumfahrt, Rept. 2003-06, Braunschweig, Germany, 2003.

[26] Hoerner, S., *Fluid-Dynamic Drag*, Hoerner Fluid Dynamics, Bakersfield, CA, 1965.

[27] Horstmann, K. H., "Ein Mehrfach-Traglinienverfahren und Seine Verwendung fuer Entwurf und Nachrechnung Nichtplanarer Fluegelanordnungen," DLR, German Aerospace Center, Rept. FB 87-51, Braunschweig, Germany, 1987.

[28] Liersch, C., and Engelbrecht, T., "LIFTING_LINE v 2.2 Handbook," DLR, German Aerospace Center, Inst. of Aerodynamics and Flow Technology, Braunschweig, Germany, 2007.

[29] Stahl, B., and Zhai, J., "Druck- und Kraftmessungen am Halbmodell 3FF im DNW-Kryo-Kanal," Deutsch-Niederländische Windkanäle, Rept. GUK-2001C05, Cologne, Germany, 2002.

[30] Wichmann, G., Strohmeyer, D., and Streit, T., *Three-Surface-Aircraft—A Concept for Future Large Aircraft* [CD-ROM], International Council of the Aeronautical Sciences, Harrogate, England, U.K., 2000.

[31] Pfingsten, K. C., and Radespiel, R., "Numerical Simulation of a Wing with a Gapless High-Lift System Using Circulation Control," *Notes on Numerical Fluid Mechanics and Multidisciplinary Design*, Vol. 96, Springer, Berlin, 2007.

[32] Liersch, C., and Wunderlich, T., "A Fast Aerodynamic Tool for Preliminary Aircraft Design," 12th AIAA/ISSMO Multidisciplinary Analysis and Optimization Conference, AIAA Paper 2008-5901, 2008.

[33] Büscher, A., and Radespiel, R., "A Method for the Aerodynamic Analysis and Design of Nonplanar Lifting Configurations at Transonic Speeds," *Jahrbuch DGLR 1*, Deutsche Gesellschaft für Luft- und Raumfahrt, Bonn, Germany, 2003, pp. 603–612.